Analyzing electrical patterns in an experimental swine model of dyssynchrony and CRT

David Soto-Iglesias, Nicolas Duchateau, Constantine Butakoff, David Andreu, Juan Fernández-Armenta, Antonio Berruezo, Marta Sitges, Oscar Camara

Analyzing Electrical Patterns in an Experimental Swine Model of Dyssynchrony and CRT

David Soto-Iglesias[1], Nicolas Duchateau[2], Constantine Butakoff[1], David Andreu[2],Juan Fernández-Armenta[2], Antonio Berruezo[2], Marta Sitges[2], Oscar Camara[1]

[1] PhySense, DTIC, Universitat Pompeu Fabra, Barcelona, Spain
[2] Cardiology Department, Thorax Institute, Hospital Clínic, IDIBAPS, Universitat de Barcelona, Spain

Abstract

Electroanatomical maps (EAM) are currently used to visualize electrical activation patterns jointly with the patient's anatomy. However, they are intrinsically specific to each subject and suffer from the lack of a common space of coordinates in which intra- and inter-subject comparisons can be performed. We propose a method for mapping this EAM surface-based information to a common geometry (using a homeomorphic mapping to a disk) to solve this issue. By applying our methodology to EAM from an experimental swine model of left bundle branch block (LBBB) dyssynchrony, we show that this provides insights into (i) the changes in electrical patterns induced by LBBB and (ii) the extent, to which consecutive resynchronization is able to restore such patterns. Analyzing the experimental data with our methodology, we demonstrate that CRT not only partially restores the global activation but also the local activation patterns, which had been degraded by the induction of LBBB.

1. Introduction

Cardiac resynchronization therapy (CRT) is a treatment for congestive heart failure aiming at correcting the electrical activation of the heart and making the heart contract synchronously. However, the high rate of non-responders to CRT (about 30%) and associated costs, make the task of selecting appropriate patients who would benefit from the therapy critical [1].

In order to better understand the mechanisms behind cardiac pathologies involving electrical abnormalities and to correct their effects, electro-anatomical maps (EAM) provided by electrophysiological mapping systems are currently used in clinical practice (see Figure 1.a and 1.b for an example). They allow for a detailed analysis of cardiac activation patterns by linking the local electrical activation (given by intracardiac electrograms) with the anatomy. These patterns may be of particular interest in order to study electrical abnormalities involved in cardiac arrhythmias or the mechanisms responsible for specific types of dyssynchrony such as left bundle branch block (LBBB), which may highly condition CRT response [2].

In this paper we present an analysis of baseline, LBBB- and CRT-induced changes in the activation patterns of an experimental swine model (N=10) of LBBB-induced dyssynchrony, implanted with a CRT device [3]. The analysis is carried out by mapping the acquired data into a common geometry, by a methodology described elsewhere [4, 5]. In short, we map the electrical activation information contained in each EAM onto a 2D disk using a homeomorphism between any ventricular surface and this disk. This disk mapping strategy is quite common in clinical cardiology when displaying acquired measurements on a bull's eye plot (BEP) representation. The proposed mapping methodology allows for statistical comparisons at each anatomical location, which in the context of our application consist of intra- (baseline vs LBBB and CRT) and inter-subject comparisons. Additionally, the high variability in initial and final activation times requires this information to be normalized, e.g. between 0 and 100 % values, prior to any intra- and inter-subject statistical comparison.

2. Materials

2.1. Protocol

A total of 10 pigs (weight = 34 (30/35) kg) [1] with no structural disease were studied in the present paper, a subpart of a larger dataset [3]. This particular sub-population was considered in order to focus on pure LBBB-induced electrical patterns and the performance of CRT in the absence of additional factors, such as local infarct.

[1]Median (1st/3rd quartile). Quantitative variables were expressed as median-interquartile range due to the limited number of samples (N=10).

Animal handling was approved by the Institutional Review Board and Ethics Committee at Hospital Clínic, Barcelona, Spain, and conformed to international guidelines [6].

LBBB was induced in all animals using radio-frequency ablation, assisted by high rate pacing (160bpm) during the burning process to prevent ventricular fibrillation. All the pigs received a RV apical lead (Beflex RF45, Sorin Group, Milan, Italy) and a LV one (subxiphoid access or via coronary sinus, Situs OTW, Sorin Group). Pacing was performed with a pacing system analyzer (ERA-3000, Biotronik, Berlin, Germany), and optimized after the ablation procedure. Further details about the protocol can be found in [3].

The ablation protocol resulted in 5 (3/13) burnings, at 25mW during 30s. QRS width significantly increased from baseline to LBBB (baseline: 55 (50/57) ms; LBBB: 84 (78/88) ms, p=0.005).

2.2. Acquisition of electro-anatomical maps

Contact mapping data was collected with an electro-anatomical mapping device (CARTO-XP, Biosense Webster, Diamond Bar, CA) after introducing a quadripolar catheter through the femoral vein until reaching the endocardium (endocardial EAM).

EAMs were subsequently generated by reconstructing information obtained from the set of sparse acquisition points where the clinician placed the catheter to measure the electrical activity (around 2500ms at 1kHz). These electrical measurements were processed and rendered in 3D to display the Local Activation Time (LAT), as shown in Figure 1.a and 1.b. The LAT is the parameter retained in the present study to investigate electrical activation patterns. All maps were acquired on the day of the experiment, at baseline, post-ablation (LBBB) and with CRT pacing, and the averaged contained points were 171 ± 66 and 255 ± 76, for endocardium and epicardium respectively.

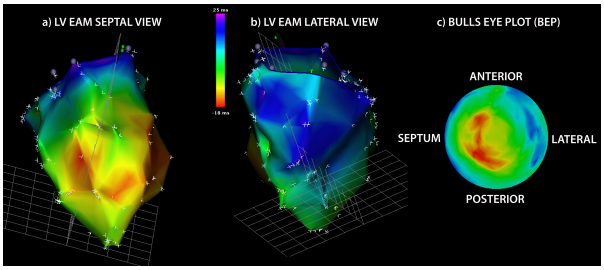

Figure 1. a).Left ventricle EAM Septal view. b). left ventricle EAM lateral view c). Projection onto a disk.

3. Methods

3.1. Homeomorphic mapping to a disk

The endocardial surfaces have a form of a cut ellipsoid and are homeomorphic to a disk. This homeomorphism can be calculated by requiring that every vertex coordinate of the triangulation has a vanishing Laplacian, as we proposed in [4, 5].

Let $\varphi : M \to D \subset R^2$ be the sought bijective mapping between the surface M and a unit disk D, ∂D – a boundary of of D, ∂M – a boundary of M.

For simplicity, let us assume that the disk is in the XOY coordinate plane, and the boundary coordinates are given by vector-columns x_0 and y_0 (concatenation of x and y coordinates of all boundary points). Let $\mathbf{L}_{M\setminus\partial M}$ be the Laplacian matrix of the mesh for surface M with the rows corresponding to its boundary ∂M removed. Let $\mathbf{x}_{\partial D}$, $\mathbf{y}_{\partial D}$, $\mathbf{x}_{D\setminus\partial D}$ and $\mathbf{y}_{D\setminus\partial D}$ be the $\mathbf{x}$, $\mathbf{y}$ coordinates of the points on the disk (the ones which we are calculating and that define our mapping) corresponding to the boundary and the interior, respectively. Then, the solution to the following two systems of linear equations give the desired mapping φ (defined by triangulation with vertices $\mathbf{x}$ and $\mathbf{y}$, with connectivity retained from the mesh representation of M [7]):

$$\begin{cases} \mathbf{L}_{M\setminus\partial M} \cdot \mathbf{x}_{D\setminus\partial D} = 0 \\ \mathbf{x}_{\partial D} = \mathbf{x}_0 \end{cases}; \begin{cases} \mathbf{L}_{M\setminus\partial M} \cdot \mathbf{y}_{D\setminus\partial D} = 0 \\ \mathbf{y}_{\partial D} = \mathbf{y}_0 \end{cases} \quad (1)$$

The above map still has two issues: the apex is not necessarily mapped to the disk's center and there is an orientation ambiguity due to the symmetry of the ventricle. In order to produce a meaningful mapping, two more points need to be defined: apex and one reference point (mid septum at the height of the mitral annulus). The reference point is mapped to the point $(-1, 0)$ of the disk's circumference and thin plate splines are used to map the apex to the point $(0, 0)$ (the center of the disc). This disk is used as a common reference frame for all the left ventricles in the EAM dataset. Since each endocardial surface has a different parametrization (different number of vertices, distributed differently), we also need to define a common disk parametrization (set of vertices and connectivity). These vertices are generated as intersection points of concentric circles of increasing radius and rays emanating from the disk's center.

3.2. Data Analysis

The experimental protocol generates different activation maps for each case, corresponding to the different stages (baseline, LBBB, CRT), all having distinct patterns, point

density and starting/ending activation times. Such differences require normalization of the activation times to a common scale prior to any intra- and inter-subject comparison. For every EAM, LAT is scaled between 0 and 100% of the maximum LAT, preserving information of left ventricle total activation time (LVTAT). The output of this operation is a set of spatio-temporally normalized activation maps, which serve for the analysis of local activation patterns. Additionally, the percentage of activated tissue is computed from each of these maps, as global measure of activation, to complement local observations.

Only non-parametric statistical tests were used due to the limited number of samples (N=10). Wilcoxon signed-rank test was used for paired data comparison. p-value < 0.05 were considered as a statistically significant difference between the tested groups.

4. Results

Median-interquartile range for left ventricle initial activation time (LV-IAT), left ventricle final activation time (LV-FAT) and left ventricle total activation time (LV-TAT) are shown in Table 1. Differences in these three activation time parameters between the different experimental stages (baseline vs. LBBB; baseline vs. CRT; LBBB vs. CRT) were all statistically significant ($p< 0.05$), except for LV-TAT between LBBB and CRT.

Table 1. Median (1st/3rd quartile) values, for left ventricle initial activation time (LV-IAT), left ventricle final activation time (LV-FAT) and left ventricle total activation time (LV-TAT) at baseline, LBBB and CRT states.

ms	LV-IAT	LV-FAT	LV-TAT
baseline	-16 (-23/-14)	23 (14/32)	44 (35/48)
LBBB	-35 (-46/-17)	37 (29/46)	65 (56/84)
CRT	16 (8/20)	82 (64/95)	65 (49/73)

In order to compare the electrical activation patterns in the different experimental stages, all the EAM have been mapped onto the common reference 2D geometry (disk) using the methodology describe in Section 3.1. Once in a common reference system with correspondence, it is trivial to compute statistics. Median-interquartile range statistics of local activation maps at baseline, LBBB and CRT stages were obtained, as illustrated in Figure 2 where one can observe the different local electrical activation patterns.

In addition, we have estimated the global electrical activation pattern as a percentage of activated tissue over time (being 0 the LV-IAT and 100% the LV-FAT). Median-interquartile range graphs have been integrated over all cases, as shown in Figure 3.

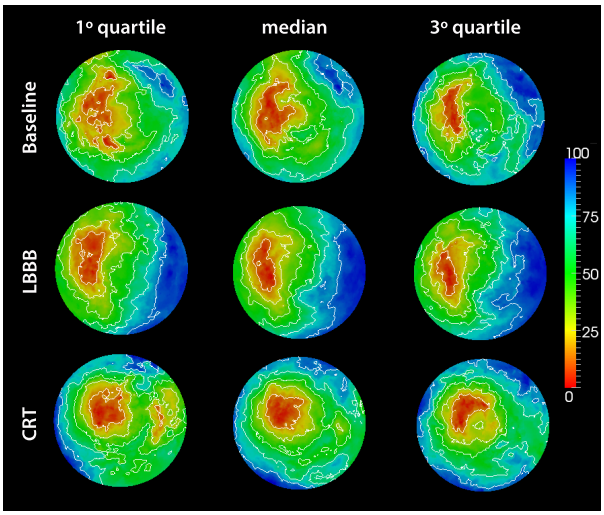

Figure 2. Disk maps of median-interquartile range (1st-3rd) with 10ms isochrones for the three baseline, LBBB and CRT states. Red colour represents earlier activation times; blue colour represents last activation times.

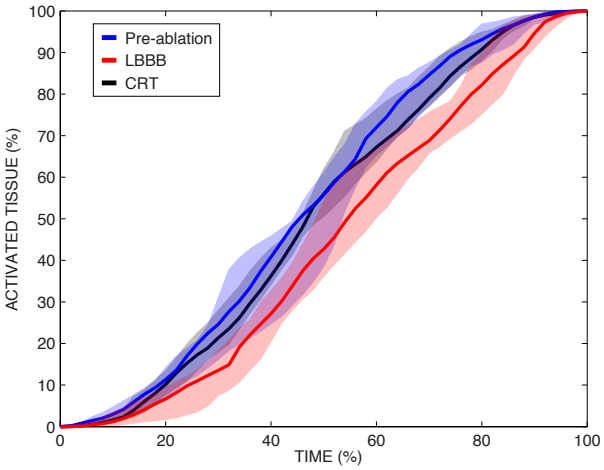

Figure 3. Median (lines) and interquartile range (shadow areas) of %activated tissue vs %time, for baseline (blue), LBBB (red) and CRT (black).

5. Discussion

As can be seen in Table 1, no significative differences in LV-TAT were observed between LBBB and CRT stages. This is probably due to the fact that population-based analysis may hide different individual behaviors. Indeed, almost no changes between LBBB and CRT in LV-TATs were observed in 3 cases (2 (1.25/3.50) ms), while CRT considerably reduced (i.e. improved) the LV-TAT in 5 cases (16 (9.75/23) ms), while in the last 2 cases the CRT LV-TAT were increased (i.e. worsened) (15 (15/15) ms). This high variability in the activation times also suggests

that a normalization from 0 to 100% is needed.

Delay in the early activation can be seen for the LBBB stage as compared to baseline (red line, LBBB, versus blue line, baseline, in Figure 3), mainly after around 30% of LV-FAT. Besides, the low inter-subject variability of the LBBB global activation indicates the high reproducibility of the observations induced by the ablation performed. Finally, almost complete recovery of the global activation pattern after CRT is observed (black line in Figure 3). The relatively high variability in baseline and CRT global activation patterns is partially explained by the local measurements displayed in Figure 2, which show variability in the activation location (baseline) and the LV lateral lead position (CRT).

Disk maps (i.e. bull's eye plots representations) of local activation provide useful information about the location of initial and final activation times, and the way the activation pattern propagates that are difficult to obtain from clinically-used EAMs. As can be seen in Figure 2, the baseline activation pattern starts at the mid septum. Furthermore three different initiation spots are observed in the first quartile disk (apical septal, mid anteroseptal and mid posteroseptal), which is likely to be caused by the Purkinje system. At baseline, the electrical propagation is faster and more uniform, and starts from these Purkinje-originated points until the basal anterolateral area. In contrast, at LBBB, the initial activation is located in the same area, but it can be observed how this area remains uniform in the first quartile, which may reflect that the electrical activation is not induced by the Purkinje system at LBBB but rather comes from the right ventricle. This causes a propagation front, from septal to lateral wall, which in the disk representation is aligned with the vertical direction (as shown in Figure 2). Finally, after CRT, one can observe the partial restoration of the local activation pattern, which gets closer to the baseline stage. Note that due to the statistics we used, differences in the lead position may not be fully visible (median disk), but observations of other quartiles can still allow to observe these differences (first and third quartiles to better distinguish earlier and last activation times, respectively).

6. Conclusions

In this work we presented a methodology for mapping LV shapes into a common geometry, which allows to compare the electrical activation patterns of a same individual at different stages and of different individuals. We shown that temporal normalizing is necessary to overcome the limits of simple non-normalized activation times measurements, and additionally focus on the differences in the initiation / end activation locations and propagation speed.

Finally, the computation of statistics over the whole population also allows to estimate the variability of the experimental protocol (apparition of LBBB specific pattern post-ablation) and the clinical hypothesis to be tested (pure LBBB in the lack of structural disease are likely to recover a normal electrical activation).

Further work is required to link this electrical information with mechanical (dys)synchrony and therefore the global heart performance at the different stages studied in the experiment.

Acknowledgements

This study was partially founded by the Spanish Ministry of Science and Innovation (TIN2011-28067) and the Spanish Industrial and Technological Development Center (cvREMOD-CEN-20091044). The authors gratefully acknowledge the support of N Solanes, M Rigol, E Silva, A Doltra, L Gabrielli, L Mont, J Brugada (Hospital Clínic, Barcelona, Spain) and A Barcelo (Sorin Group, Barcelona, Spain) on the experimental protocol.

References

[1] Bleeker G, Bax J, Fung J, et al. Clinical versus echocardiographic parameters to assess response to cardiac resynchronization therapy. Am J Cardiol 2006;97:260–3.

[2] Duckett S, Camara O, Ginks M, et al. Relationship between endocardial activation sequences defined by high-density mapping to early septal contraction (septal flash) in patients with left bundle branch block undergoing cardiac resynchronization therapy. Europace 2012;14:99–106.

[3] Rigol M, Solanes N, Fernandez-Armenta J, et al. Development of a swine model of left bundle branch block for experimental studies of cardiac resynchronization therapy. Journal of Cardiovascular Translational Research 2013;In press.

[4] Soto-Iglesias D, Butakoff C, Andreu D, et al. Evaluation of different mapping techniques for the integration of electro-anatomical voltage and imaging data of the left ventricle. In FIMH'13, LNCS 7945. 2013; .

[5] De Craene M, Tobon-Gomez C, Butakoff C, et al. Temporal diffeomorphic free form deformation (TDFFD) applied to motion and deformation quantification of tagged MRI sequences. volume 7085. 2012; 68–77.

[6] Committee for the Update of the Guide for the Care and use of Laboratory Animals; National Research Council. Guide for the Care and Use of Laboratory Animals. Eighth edition edition. The National Academies Press, 2011.

[7] Tutte W. How to draw a graph. Proceedings of the London Mathematical Society 1963;13(3):743–768.

Address for correspondence:

Name David Soto Iglesias

Full postal address Carrer Tanger, 122-140, 08018 Barcelona,Spain

E-mail address david.soto@upf.edu(optional)